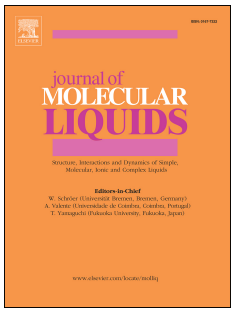

Covalent triazine-based polyimine framework as a biocompatible pH-dependent sustained-release nanocarrier for sorafenib: An in vitro approach

Nazanin Mokhtari, Somayeh Taymouri, Mina Mirian, Mohammad Dinari

PII: S0167-7322(19)34556-8

DOI: https://doi.org/10.1016/j.molliq.2019.111898

Reference: MOLLIQ 111898

To appear in: *Journal of Molecular Liquids*

Received Date: 13 August 2019

Revised Date: 6 October 2019

Accepted Date: 10 October 2019

Please cite this article as: N. Mokhtari, S. Taymouri, M. Mirian, M. Dinari, Covalent triazine-based polyimine framework as a biocompatible pH-dependent sustained-release nanocarrier for sorafenib: An in vitro approach, *Journal of Molecular Liquids* (2019), doi: https://doi.org/10.1016/j.molliq.2019.111898.

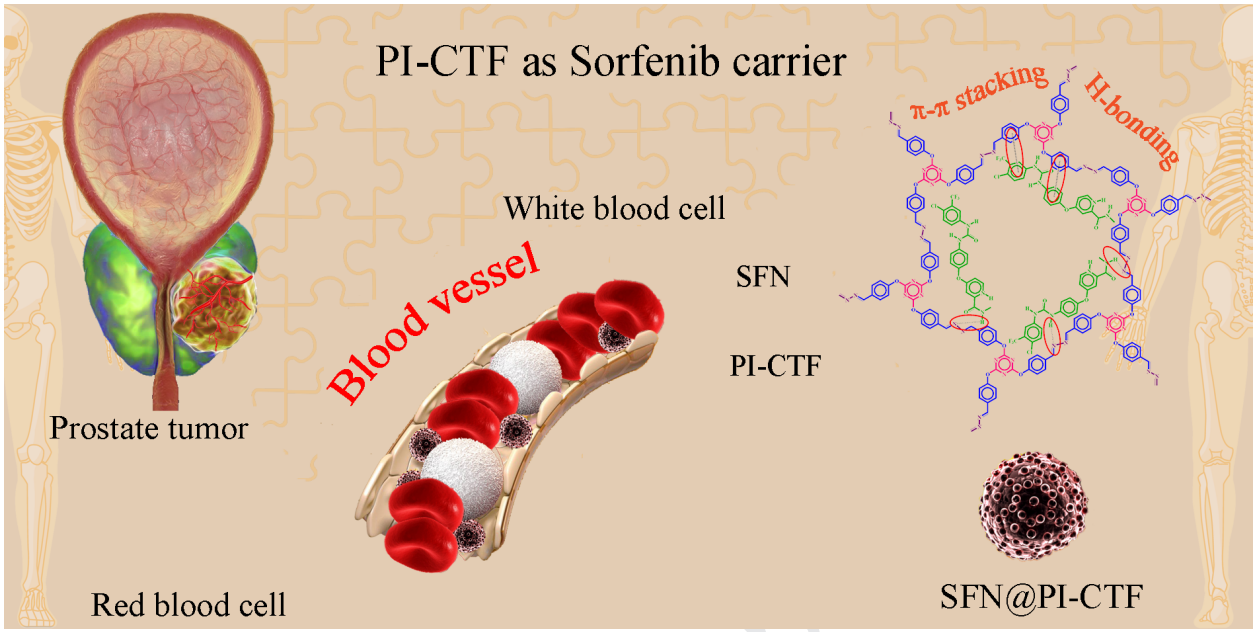

Revised

Covalent triazine-based polyimine framework as a biocompatible pH-dependent sustained-release nanocarrier for Sorafenib: an in vitro approach

Nazanin Mokhtari [a], Somayeh Taymouri [b], Mina Mirian[c], and Mohammad Dinari[1] [I, a]

[a] Department of Chemistry, Isfahan University of Technology, Isfahan, 84156-83111, Islamic Republic of Iran.

[b] Department of Pharmaceutics, School of Pharmacy and Novel Drug Delivery Systems Research Centre, Isfahan University of Medical Sciences, Isfahan, Iran.

[c] Department of Biotechnology, School of Pharmacy and Pharmaceutical Sciences, Isfahan University of Medical Sciences, Isfahan, Iran.

[1]Corresponding author. Tel.: (+98) 31 3391 3270; fax: (+98) 31 3391 2351.
E-mail address: dinari@cc.iut.ac.ir; mdinary@gmail.com

Abstract:

In the present study, a novel polyimine-based covalent triazine framework (PI-CTF) was introduced as a promising biocompatible carrier for sorafenib (SFN) delivery. High specific surface area and porosity allowed us to achieve drug loading and encapsulation efficiency as high as 83% and 98 %, respectively. The in vitro drug release study of SFN-loaded PI-CTF showed a sustained and pH-dependent release behavior in which acidic pH accelerated drug release compared with the neutral pH. Notably, cytotoxicity assay against L929 cells revealed the safety and biocompatibility of PI-CTF. Moreover, MTT assay against LNCaP prostate cancer cells expressed that the anticancer activity of SFN had no diminution after incorporating into PI-CTF. Thus, PI-CTF has envisaged as a great promise toward anti-cancer drug carrier.

Keywords: Covalent triazine-based framework, CTF, Sorafenib, Drug delivery, Drug controlled release.

1. Introduction:

Cancer is a result of the uncontrolled proliferation and rapidly spreading of abnormal cells to other body parts and is responsible for an estimated 13.1 million deaths in 2030 [1]. The treatment options for cancer therapy consist of surgical intervention, chemotherapy, and radiation therapy or a combination of these options [2]. Chemotherapeutic agents are non-selective and have an unfavorable bio-distribution which causes severe side effects in healthy normal tissues and preliminary stop of chemotherapy. Besides all the drawbacks of chemotherapy for cancer treatment, it is still known as one of the most acceptable and effective approaches for tumor therapy. Therefore, to decrease the side effects of anticancer drugs and

improve their efficacy, drug delivery systems should be designed with the capability of delivering the drugs to specific targets and provide sufficient concentration during a particular time [3]. Nano-based drug delivery systems are desirable as drug carrier because of their ability to carry loaded therapeutic agents into targeted organs selectively utilizing the unique pathophysiology of tumors with compromised leaky vasculature. In contrast to normal vessels with the tight endothelial junctions, the size of the fenestrations between the leaky cancer endothelium is about 100 to 780 nm which depends on the type of tumor. As a consequence, nanoparticles with suitable size have the potential to pass through the gap of the leaky endothelial cells by passive diffusion and since the tumor lymphatic system is deficient, they selectively accumulate in tumor tissue by enhanced permeation and retention (EPR) effect [4].

Among nanoparticles in development, porous organic polymers (POPs) are receiving growing interest in the last decades due to structural diversity, high surface area, and controllable porosity [5-7]. POPs are a large class of nanostructures used for various purposes in different branches of science such as catalysis, gas storage, coatings, etc. [5, 8-11]. Different kinds of classifications were reported for POPs, but generally, covalent triazine-based frameworks (CTFs) emerge as the most important structures among other categories. These structures are consisting of covalently bonded carbon and nitrogen which is led to higher chemical stability in different conditions in comparison to metal-organic frameworks (MOFs) which are more common in drug delivery systems [12]. CTFs are often synthesized by reversible condensation reactions between multi-functional aromatic amines and aldehydes. The formation of strong π-π stacking interactions between the oligomers and monomer in an error-correction crystallization is believed to be the driving force of these reactions [13]. Reversible bond linkages not only provide the capability of an error-correction and defect healing process but simultaneously make

CTFs as biodegradable materials. [14] Moreover, magnificent features such as high thermal and chemical stability, high surface area, and high porosity, undoubtedly, provide CTFs a good opportunity to be used in the biomedical fields. Recently, Bai and co-workers reported a three-dimensional CTF for 5-fluorouracil (5-FU) with high drug loading and efficient drug release behavior [15].

Sorafenib is a vascular endothelial growth factor receptor and multikinase inhibitor. It has demonstrated extraordinary anticancer effects both *in vitro and in vivo* against a wide range of tumors, including hepatocellular carcinoma [16, 17], non-small cell lung carcinoma [18], breast cancer [19], malignant melanoma [20], etc. FDA approves sorafenib for the treatment of renal cell carcinoma, unrespectable hepatocellular carcinoma and differentiated thyroid cancer [21, 22]. Several clinical studies also have reported benefits following treatment with sorafenib in prostate cancer patients [23]. However, its clinical application is greatly hampered by its undesirable systemic toxic effects such as skin toxicity, diarrhea, hypertension, fatigue, alopecia, anorexia, coronary artery spasm, and gastrointestinal bleeding and variation in pharmacokinetics resulted from low solubility [24]. Thus, several nanoparticulate systems were developed to improve its therapeutic efficacy [21]. However, to the best of our knowledge, no attempt has yet been made to use the CTFs as a carrier for sorafenib delivery.

In this work, a novel polyimide-based CTF (PI-CTF) with high thermal and chemical stability and high surface area was designed and synthesized by a facile room-temperature condensation reaction. Then, it was used as vehicles for sorafenib delivery. The physicochemical characteristics of sorafenib loaded PI-CTF were studied in terms of particle size, encapsulation efficiency, loading efficiency, morphology, and drug release kinetics. Finally, considering the efficacy of sorafenib in prostate cancer, the antitumor activity of sorafenib-loaded PI-CTF

(SFN@PI-CTF) was studied against LNCaP cells, also, the cytocompatibility of developed PI-CTF was evaluated against L929 cells.

2. Materials and methods

2.1. Materials

Analytical pure 1,2 dichlorobenzene, acetone, dichloromethane, tetrabutylammonium bromide (TBAB), sodium hydroxide, hydrazine hydrate, ethanol, potassium dihydrogen phosphate (KH_2PO_4), potassium hydrogen phosphate (K_2HPO_4), 2,4,6-trichloro-1,3,5-triazine (cyanuric chloride), tetrahydrofuran (THF), *p*-hydroxybenzaldehyde, *N*,*N*-dimethylformamide (DMF), methanol, acetic acid, ethyl acetate and hydrochloric acid were provided from Merck (Hohenbrunn, Germany) and Aldrich Chemicals Co (Steinheim, Germany). Sorafenib (SFN) was obtained from Parsian Pharmaceutical Co (Tehran, Iran). All the materials used without further purification.

2.2. Preparation of 2,4,6-tris (4-formyl phenoxy)-1,3,5-triazine (TFPTZ)

TFPTZ was synthesized as following a procedure outlined in the literature [25]. Briefly, equivalent amounts of sodium hydroxide and p-hydroxybenzaldehyde (0.04 mol) were used to prepare a 50 mL aqueous solution. Then, a 50 mL solution of cyanuric chloride (1.84 g, 0.01 mol) and TBAB (0.020 g, 6.5×0^{-5} mol) as phase-transfer catalyst in dichloromethane were added to the first solution in a 250 mL round-bottom flask and stirred for 24h at room temperature. TLC method was used to check the completion of the reaction and after that, the biphasic solution was separated [25]. In order to purify the product, the organic phase was well washed with (10 %) NaOH (3×25 mL) and distilled water (2×20 mL). Thereafter, the remained solution was dried by anhydrous sodium sulfate, filtered, and evaporation under reduced pressure, and then it was used to get the white powdered product. For a more purified product, it was then

recrystallized in ethyl acetate to afford a light white precipitate (Scheme 1). Yield (%) = 85, m.p. (°C) = 174, FT-IR (KBr) in cm^{-1}: v = 1210 (C-O), 1370 (C-N), 1560 (C=N), 1697 (C=O), 2800-2925 (C-H aldehyde), ^{13}CNMR (400 MHz, $CDCl_3$, ppm): δ = 120-160 (C aromatic), 171 (C=N triazine ring), 180 (C=O aldehyde) (Fig. S1); elemental analysis for $C_{24}H_{15}N_3O_6$ (experimental/theoretical): C 65.03/61.35, H 3.74/3.41, N 9.42/9.59, O 21.81/21.75.

2.3. Preparation of PI-CTF

To prepare PI-CTF, 33 mg (0.08 mmol) of TFPTZ was added to a 10 mL glass vial and then it was charged with 2 mL of 1,2-dichlorobenzene/ethanol (2:3 v/v). In order to get a homogeneous dispersion, it was then sonicated for 10 min. Afterward, 6.5 μL (0.21 mmol) of hydrazine was added to the obtained suspension and it was sonicated for another 5 min. Afterward, 0.2 mL of acetic acid solution (6M) was added to the vial and it was sealed and kept undisturbed for 3 days. Finally, the obtained yellow precipitate collected by centrifugation and washed several times with anhydrous THF, anhydrous acetone, and anhydrous dichloromethane, respectively. Subsequently, anhydrous methanol was used for solvent exchange and then the activated product was dried at 120 °C under vacuum for 12h. FT-IR (KBr) in cm^{-1}: v = 998 (N-N), 1215 (C-O), 1363 (C-N), 1563 (C=N); elemental analysis for $C_{39}H_{21}N_9O_6$ (experimental/theoretical): C 62.98/65.52, H 4.25/2.98, N 18.08/17.71, O 14.69/13.42.

2.4. Characterization of PI-CTF

Moreover, PI-CTF structure was thoroughly characterized using elemental analysis, powdered X-ray diffraction (XRD), Fourier transform infrared (FT-IR) spectroscopy, field-emission electron microscopy (FE-SEM), transmission electron microscopy (TEM), thermogravimetric analysis (TGA), and CO_2 sorption, as described in the Supporting Information (SI).

2.5. Preparation of SFN@ PI-CTF

Briefly, a specific amount of SFN was dissolved in DMF and different amounts of PI-CTF (Table 1) were added into the solution. The carrier: drug ratio in the loading solution was 5:1, 1:1, 1:2 and 1:5 (wt.: wt.). Then, the mixtures were sonicated for 4h and stirred for 6-24 h at ambient temperature. After that, the mixtures were centrifuged at 6000 rpm for 10 min. The supernatant was completely removed and retained to calculate the drug-loading factors. The precipitated SFN@PI-CTF were washed with water and freeze-dried for further investigations.

2.6. Encapsulation efficiency and drug loading of SFN

The encapsulation efficiency and drug loading were evaluated UV-Vis spectrophotometrically by using the supernatant and standard solutions of SFN at 280 nm. The following equations were used to determine drug loading and encapsulation efficiency:

$$\text{Encapsulation efficiency \%} = \left(\frac{\text{the total amount of drug added} - \text{free drug}}{\text{the total amount of drug added}} \right) \times 100$$

$$\text{Drug loading \%} = \left(\frac{\text{the total amount of drug added} - \text{free drug}}{\text{the weight of SNF@ PI-CTF}} \right) \times 100$$

2.7. *In vitro* drugs release and kinetics

The release behavior of SFN from the formulation with the highest encapsulation efficiency and drug loading (Table 1, entry 1) was evaluated at 2 different pH (5.3 and 7.4). For this, an appropriate amount of freeze-dried SFN@PI-CTF was dispersed in phosphate buffer solution (PBS) and filled in a dialysis bag (molecular cut off 50 kDa) and then, the end sealed dialysis bag was immersed into the PBS (pH 5.3 and pH 7.4) containing 40% methanol at 37 ˚C. At predetermined time intervals (every 2 hours), the absorbance of the external medium was measured by using UV-Vis spectrophotometer at 280 nm to determine the drug release (Fig. 5).

The obtained release data from the designed formulation were fitted into various kinetic models such as Higuchi ($Qt = k_H t^{1/2}$), zero-order ($Qt = Q_0 + k_0 t$), Baker-Lonsdale: $[1-(1-Q_t/Q_\infty)^{2/3}]- Q_t/Q_\infty = kt$, first-order ($\ln Q_t = \ln Q_0 + k_1 t$), and Peppas model ($Q_t/Q_0 = kt^n$) [17]. In these equations, Q_0 is the initial amount of drug, Q_t is the amount of drug released at time t, t is sampling time, *k* is release constant, and n is release exponent. The best mathematical model to describe drug release from PI-CTF is the one with the highest correlation coefficient. Exponent (n) was calculated to determine the mechanism of drug release from PI-CTF. n can take the three following values: $0.5 < n < 1$, $n = 1$, and $n \leq 0.5$ that are related to the non-Fickian (anomalous drug diffusion) model, zero-order mechanism, and Fickian diffusion mechanism, respectively. n values higher than 1 indicated the super case II transport [26].

2.8 *In vitro* cytotoxicity assays

LNCaP prostate cancer cell line and L929 normal fibroblast cell line were purchased from the national bank of Iran pasture institute and cultured in RPMI1640 enriched with 10% FBS (Gibco/USA) and 1% penicillin/streptomycin (Gibco, USA) at 37°C in a humidified incubator with 5% CO_2. Then, the cytotoxicity of free SFN, free PI-CTF, and SFN@PI-CTF against LNCaP cells were estimated by MTT assay. Briefly, about 1×10^4 cells per well were incubated into 96-well plates for 24 h and then, cells were treated with a series of SFN@PI-CTF and free SFN with equivalent SFN concentration ranging from 0.25 to 10 µg/mL.

Drug-free SFN@PI-CTF was also assessed by the same concentrations as drug-loaded SFN@PI-CTF on LNCaP cells. After 48 and 72 h of incubation, the medium was discarded and 20 µL of MTT solution (5 mg/mL) was added to each well and located in 37°C for 3 h. Then, the media were replaced with DMSO (150 µL/well) to solubilize the formazan crystals. The

absorbance value for wells was evaluated at a wavelength of 570 nm using ELISA plate reader. Finally, cell viability percentages were calculated according to the following formula:

$$\text{Cell viability \%} = \left(\frac{\text{mean absorbance of sample} - \text{mean absorbance of blank}}{\text{mean absorbance of control} - \text{mean absorbance of blank}}\right) \times 100$$

Moreover, the drug-free PI-CTF cytotoxicity was measured against mouse fibroblast L929 cells by MTT assay. In summary, about 1×10^4 L929 cells plated and after 24 h treated with various concentrations of drug-free PI-CTF for 48 and 72 h and then, cell survival percentage was assessed using MTT assay.

3. Results and discussion

3.1. Synthesis and characterization

In the current study, the building block of a novel PI-CTF was synthesized through a nucleophilic substitution of *p*-hydroxybenzaldehyde and cyanuric chloride at a room temperature process. Then, the prepared monomer was used to synthesize the PI-CTF by a facile solution-suspension method at room temperature. In a typical procedure, a homogenous dispersion of TFPTZ was placed in a 10 mL vial and then the hydrazine was added and kept undisturbed for 3 days at room temperature [25]. The yielded precipitate was washed several times with anhydrous solvents and dried under vacuum (Scheme 1). Finally, the structure was confirmed by FT-IR, XRD, TGA, CHNS, TEM, FE-SEM, and CO_2 sorption.

In order to prepa

re the SFN@PI-CTF, different weight ratios of PI-CTF: SFN were used and the encapsulation efficiency and drug loading at different incubation time were investigated and the results are illustrated in Table 1. An increase in the SFN/PI-CTF accompanied by increasing the encapsulation efficiency and drug loading. Consequently, SFN/PI-CTF=5 (Table 1, entry 4)

which is prepared after 6 h incubation, found to be the optimal formulation and used for further investigation.

Table 1. Formulations and effective factors on the drug loading process

Entry	PI-CTF: Drug	Drug Loading (%)		Encapsulation Efficiency (%)	
		6 h	24 h	6 h	24 h
1	5:1	7.8	8.6	42.5	47.2
2	1:1	36.9	36.9	58.6	58.6
3	1:2	64.7	64.4	91.8	90.4
4	1:5	83.0	83.1	98.1	98.8

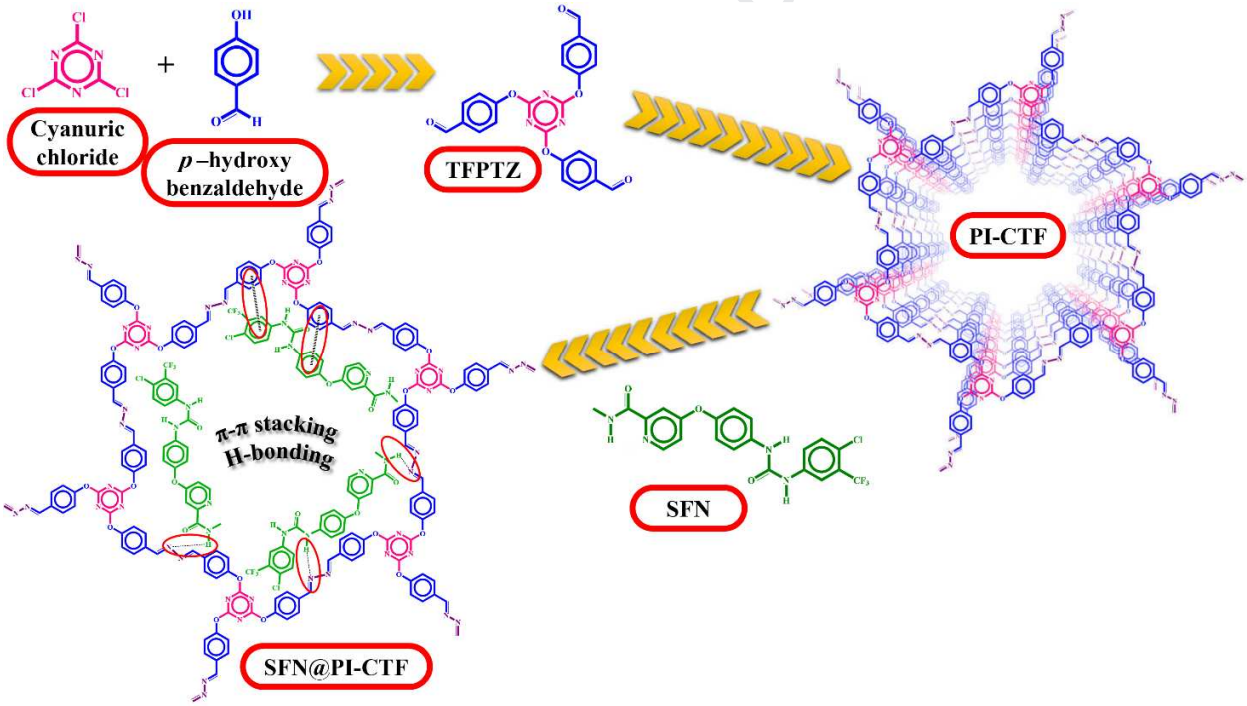

Scheme 1. A schematic illustration for preparation of PI-CTF and SFN@PI-CTF.

3.2. FT-IR study

Fig. 1(a-c) represents the FT-IR spectra of cyanuric chloride, *p*-hydroxybenzaldehyde, and the TFPTZ which is the building block of the PI-CTF structure. In the case of TFPTZ, the existence of a peak at 2800-2925 cm^{-1} shows the presence of the aldehyde C-H bond in the

structure. The C-O bond absorbance appeared at 1210 cm^{-1} and the C=N bond was shown around 1500-1600 cm^{-1}. In addition, the presence of a sharp peak at 1690 cm^{-1} represents the aldehyde carbonyl group [25]. The addition of hydrazine to TFPTZ led to form new bonds in the structure of PI-CTF. The disappearance of the carbonyl stretching frequency at 1690 cm^{-1} and formation of new bonds in the range of 990-1560 cm^{-1} are related to the presence of C=N, C-N, and N-N vibrational stretching and confirmed the structure of PI-CTF (Fig. 1 (c-e)) [27].

Possible interaction between sorafenib and PI-CTF in prepared SFN@PI-CTF was evaluated by the FT-IR study. The presence of carboxyl groups in the SFN structure led to observe strong bands at 1691 cm^{-1} and 1712 cm^{-1}. N-H group of amine and urea was detected by a single-branched peak in the region of 3146-3396 cm^{-1}. The C-F vibrational band of the $–CF_3$ group was also observed as a sharp and strong band in the region of 1006 -1314 cm^{-1}. In the case of SFN@PI-CTF, a slight red-shift was observed for carboxyl groups from 1701-1720 cm^{-1} to 1691-1712 cm^{-1} which might be related to the formation of hydrogen bonds between the amide hydrogens and carbonyl species (Fig. 1(e-g)).

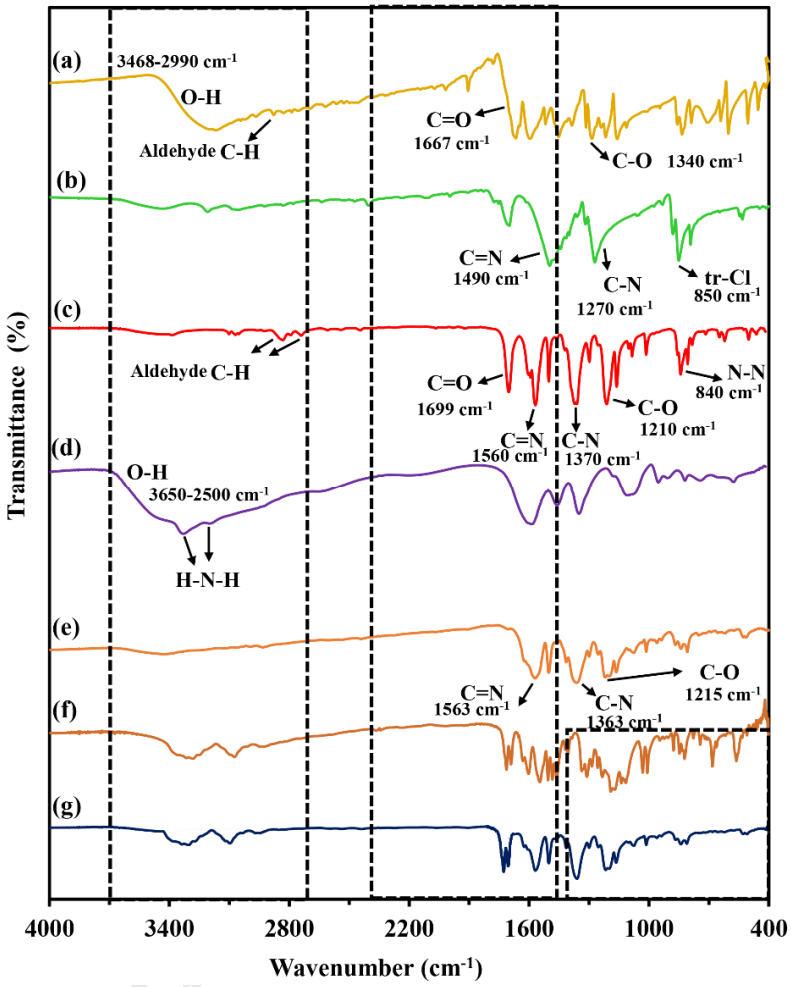

Figure 1. FTIR spectra of (a) *p*-hydroxy benzaldehyde, (b) cyanuric chloride, (c) TFPTZ, (d) hydrazine hydrate, (e) PI-CTF, (f) SFN, (g) SFN@PICTF.

3.3. XRD study

The x-ray diffraction pattern of PI-CTF was also studied to investigate the crystalline nature of the CTF. Two peaks were seen in the obtained XRD pattern, a strong peak at 3.2˚ and a relatively weak band at 5.9˚ (Fig. 2). The regularly arranged crystalline structure of PI-CTF could help to increase loading factors.

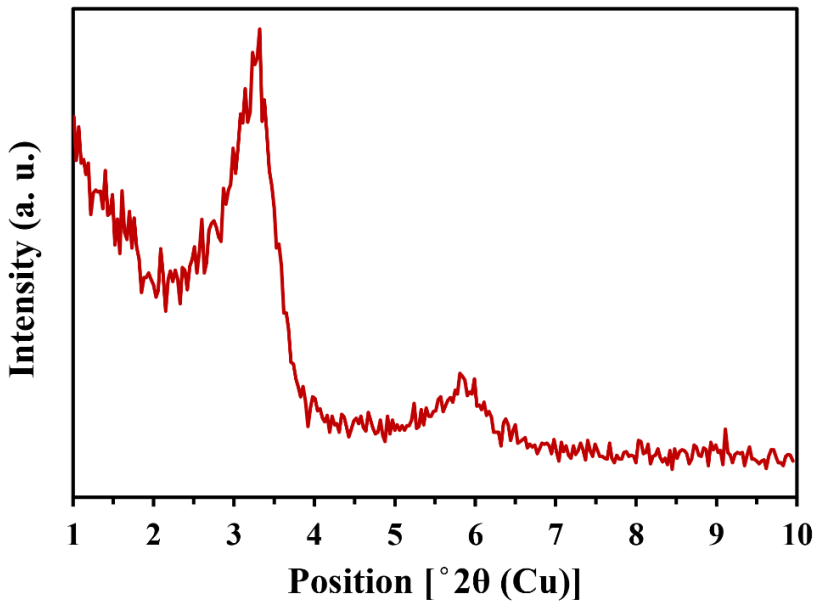

Figure 2. XRD pattern of TFPTZ**.**

3.4. TGA study

TGA is a reliable means for the investigating compounds thermal properties. Herein, the obtained thermogram was expressed high thermal stability (Fig. 3a). The thermal stability of a sample usually determines by studying the decomposition temperatures of 5% and 10% of the compound, char yield at 800 ˚C, and also the limiting oxygen index (LOI). LOI of PI-CTF was calculated by the Van Krevelen and Hoftyzer equation and were summarized in Table 2 [28].

$$LOI = 17.5 + 0.4\ CR$$

Where CR stands for char yield. Thus the PI-CTF can be stable at about 350 ˚C might be due to the presence of aromatic rings. According to previous studies [29-31], PI-CTF can be put in the classification of self-extinguishing materials. The LOI value of PI-CTF was decreased after SFN incorporation which is attributed to the lower thermal resistance of SFN in the SFN@PI-CTF structure. Incorporation is a proper solution for rising stability against oxidation.

Table 2. Comparison of thermal properties of the PI-CTF and free SFN

Samples	$T_{dec}^{\%5}$	$T_{dec}^{\%10}$	Char yield (%)	LOI
PI-CTF	363	435	54	39.1
SFN@PI-CTF	319	379	40	33.5
SFN	250	271	25	27.5

TGA curves of PI-CTF, SFN@PI-CTF, and SFN are also shown in Fig. 3. The comparison between curve (a) and curve (b) reveals lower thermal stability of SFN@PI-CTF which is mainly resulted from the SFN decomposition (curve (c)) and its mass loss at lower temperatures. Moreover, the comparison between curve (b) and curve (c) expressed that the SFN decomposition is prevented by incorporating into the PI-CTF hollow structure. [32].

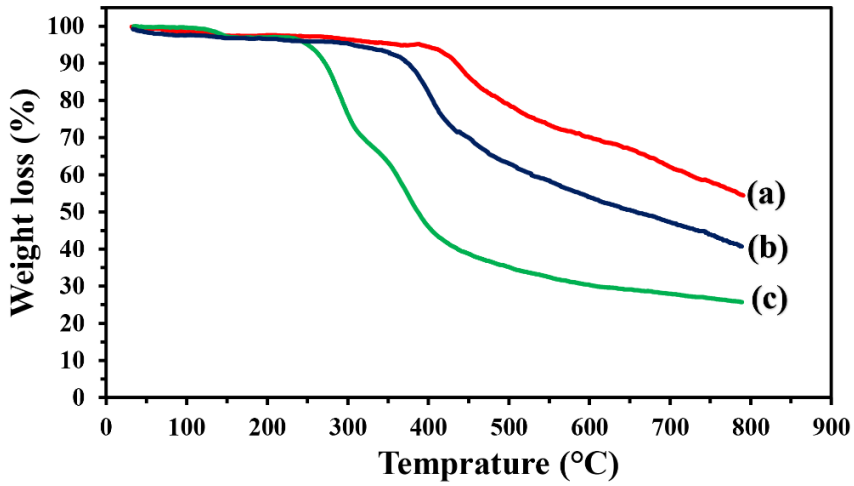

Figure 3. TGA curves of (a) PI-CTF, (b) SFN@PI-CTF, (c) SFN

3.5. Morphological study (FE-SEM and elemental mapping)

The FE-SEM micrographs show a structure similar to that observed in marine corals which consists of tubular structures with a diameter range of 20-40 nm and an average particle diameter of about 30 nm (Fig. 4 (a-c)). The condensation of hydrazine and TFPTZ provides a certain

degree of regularity. A small amount of freeze-dried SFN@PI-CTF was used for FE-SEM. As illustrated in Fig. 4 (e and d), no significant changes were observed in the PI-CTF morphology during drug loading, however, structural pores appear to be filled which is evidence for SFN loading. Mapping images of SFN@PI-CTF show the presence of carbon, nitrogen, oxygen, chlorine, and fluorine in the structure. C, N, and O are presented in both PI-CTF and SFN structure, in contrast, Cl and F are only found in SFN structure. Consequently, SFN was successfully incorporated into the PI-CTF structure (Fig. S2). Moreover, the EDX spectrum of SFN@PI-CTF also corroborates the obtained data from mapping images (Fig. S3).

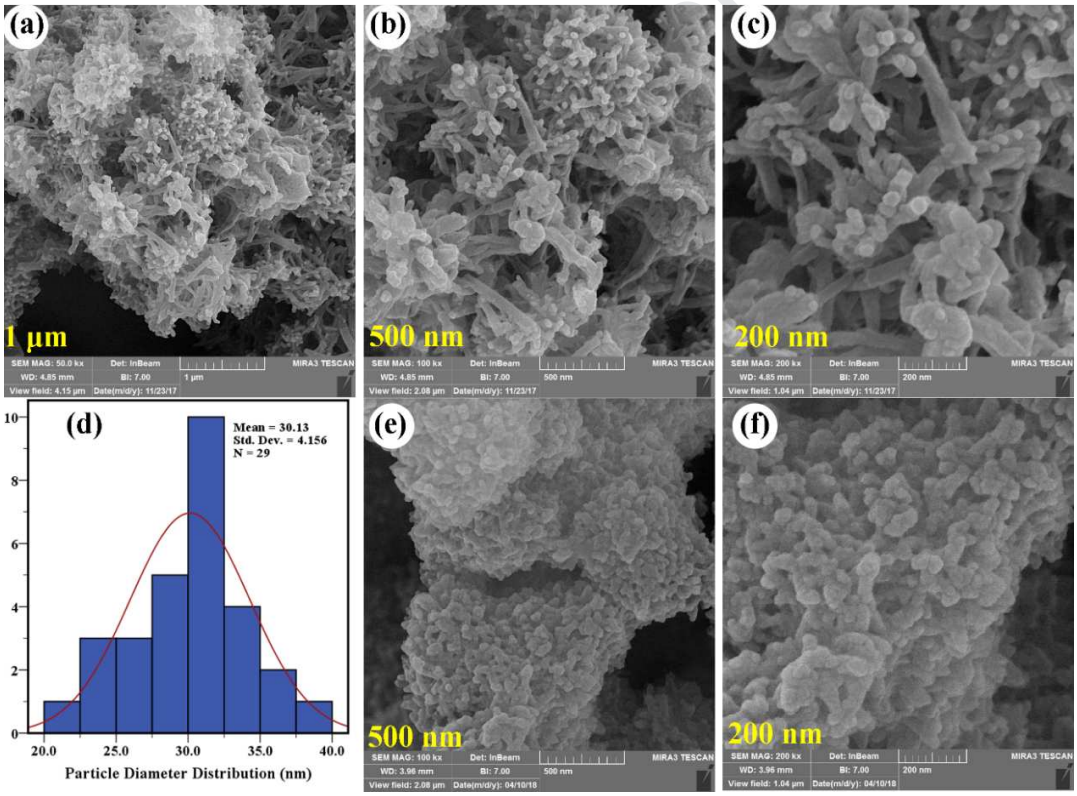

Figure 4. FE-SEM images of PI-CTF in the scale of 1µm (a), 500 nm (b), 200 nm (c), particle diameters distribution diagram of PI-CTF (d); The FE-SEM images of SFN@PI-CTF in the scale of 500 nm (e), and 200 nm (f).

3.6. CO_2 sorption study

One of the key parameters of a drug delivery systems is good drug-loading capacity which is attributed to the specific surface area, where a higher surface area could increase the loading factors [33, 34]. CTFs like other similar structures mostly consist of micropores in their structure. This phenomenon restricted the use of CO_2 instead of N_2 due to the lower kinetic diameter. Carbon dioxide adsorption study conducted at 273 K, as expressed in Table 3, the surface area of PI-CTF and the median pore width were 856 m^2. g^{-1} and 0.63 nm, respectively.

Table 3. PI-CTF surface area based on CO_2 sorption

Measurement method	PI-CTF
Dubinin-Astakhov surface area (g/m^2)	856
Langmuir surface area (g/m^2)	302
(g/cm^3) median pore width	0.63

3.7. Study of *in vitro* release and kinetics

The *in vitro* release profiles of SFN from PI-CTF in PBS at pH 5.3 and 7.4 are shown in Fig. 5. As shown in this figure, the drug release was remarkably affected by pH and increased when the pH decreased from 7.4 to 5.3. For instance, after about 48 h, SFN sustained-release from PI-CTF found to be nearly 48% and 66% at pH 7.4 and pH 5.3, respectively. This could be due to protonation of nitrogens of PI-CTF structure in an acidic condition which in turn weaken SFN-PI-CTF hydrogen bonds and results in faster SFN release [35]. The pH of the tumor extracellular region is slightly more acidic (pH 6.5 to pH 6.9) than physiological pH of normal tissue (7.2 to 7.5) possibility due to the higher rate of glycolysis in cancer cells to provide the energy needed for survival by transforming glucose into lactic acid. At the cellular level, the intracellular acidic components (pH ~5.5 for endosome, pH ~5.0 for lysosome) can also be used to trigger drug release if the nanoparticles are pH-sensitive [36].

This increase in drug release at pH 5.3 demonstrating facilitated drug release from PI-CTF in acidic endosomes and/or lysosomes (pH 4.0–6.0) after internalization in tumor cells. This result was in accordance with the results reported by Varshosaz et al [37].

The release profiles were also biphasic with a burst release followed by a slower release. Dissolution and diffusion of SFN that absorbed on the PI-CTF surface resulted in burst release which can inhibit the growth of cancer cell on the first hours of administration. Whereas, the latter is related to the diffusion of SFN from the interior hollow pores of the PI-CTF structure [38]. This phenomenon is also seen in other polymer-based structures [38-41].

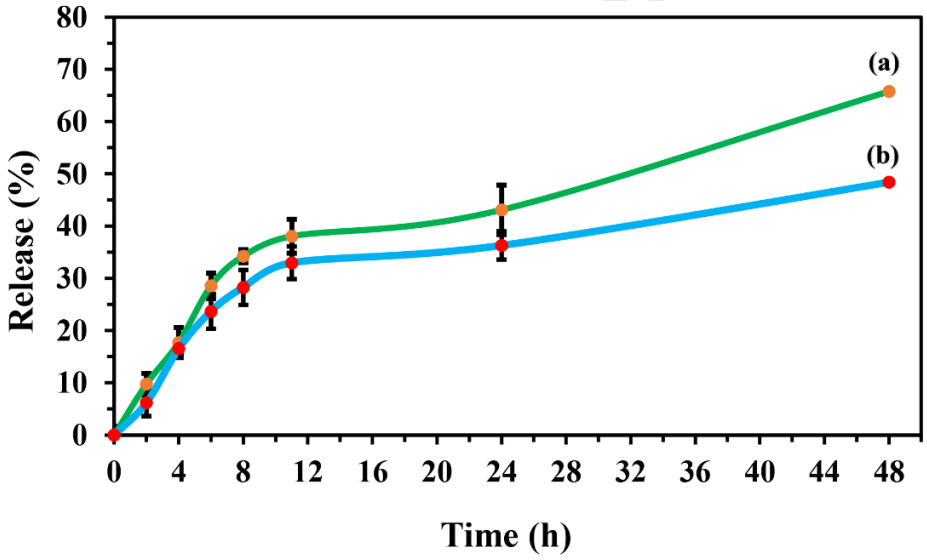

Figure 5. SFN release profile from PI-CTF in (a) pH=5.3, (b) pH=7.4.

The obtained release data from the designed formulation were fitted into various kinetic models. Based on higher R^2 values, SFN release data fitted better with Baker Lonsdale model [42] (Table 4). The mechanisms of drug release from prepared optimized PI-CTF was also evaluated using the Korsmeyer-Peppas model. Calculated release exponent was found to be between 0.5 and 1 representing both diffusion and erosion mechanisms play role in SFN release from PI-CTF (non-Fickian diffusion mechanism).

Table 4. Regression coefficient (r^2) of Sorafenib release data from PI-CTF to the different kinetic models

Samples	pH	Baker–Lonsdale	Higuchi	First-order	Zero-order	Korsmeyer-Peppas	N
PI-CTF	5.3	0.9645	0.9328	0.9341	0.8574	0.9053	0.56
PI-CTF	7.4	0.9405	0.8768	0.8340	0.7566	0.8266	0.57

3.8. *In vitro* cytotoxicity assay

The cytotoxic effects of drug-free PI-CTF on L929 cells after 48 and 72 h were reported in Fig. 6. As shown in this figure, not only PI-CTF was non-toxic against L929 cell but also increase the proliferation rate of cells in special concentrations (0.5-15 ppm and 0.5-1 ppm after 48 and 72 h, respectively). This result indicates these nanocarriers are safe and biocompatible structures and are suitable for *in vivo* antitumor drug delivery.

The *in vitro* cytotoxic activity of free SFN, SFN@PI-CTF was tested against LNCaP cells using MTT assay after 48 and 72 h exposure and the results are shown in Fig. 7a and Fig. 7b. According to these results, SFN and encapsulated SFN inhibited proliferation of LNCaP cells in a dose and time-dependent manner, but there was no significant difference in cytotoxicity of SFN and SFN@PI-CTF after 48 and 72 h incubation ($P > 0.05$). This probably would be related to the simple diffusion of free SFN into LNCaP cells which in turn cause a rapid effect on the cells. But uptake of SFN@PI-CTF is time-consuming and then, the drug will be released in a controlled manner. This finding is in accordance with the results in the other literature employing anticancer drug-loaded nanoparticles where free drug illustrated higher cytotoxicity than drug-loaded nanoparticles[43-50]. In addition to SFN@PI-CTF and free SFN, the cytotoxic effect of drug frees PI-CTF, in the equivalent concentration as used for SFN@PI-CTF was also investigated. Fig. 7a and Fig. 7b showed drug-free PI-CTF were non-toxic against LNCaP cells in low concentrations, but, a little toxicity was seen with cell viability of near 70% in high concentration.

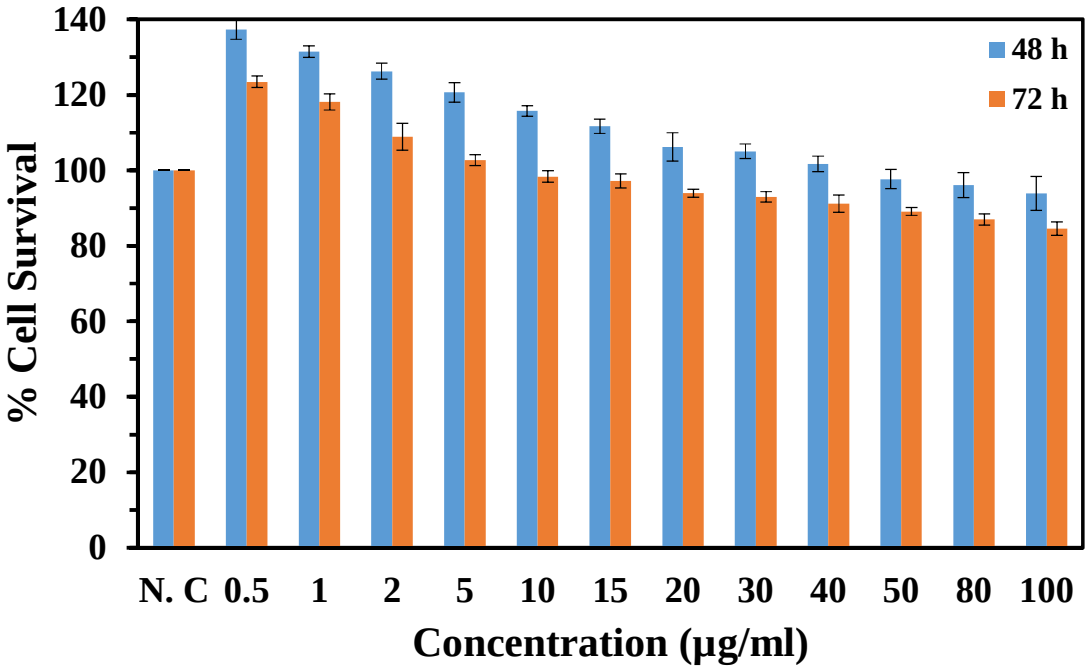

Figure 6. Cytotoxicity of PI-CTF against L929 cells after 48 and 72 h, N.C; negative control.

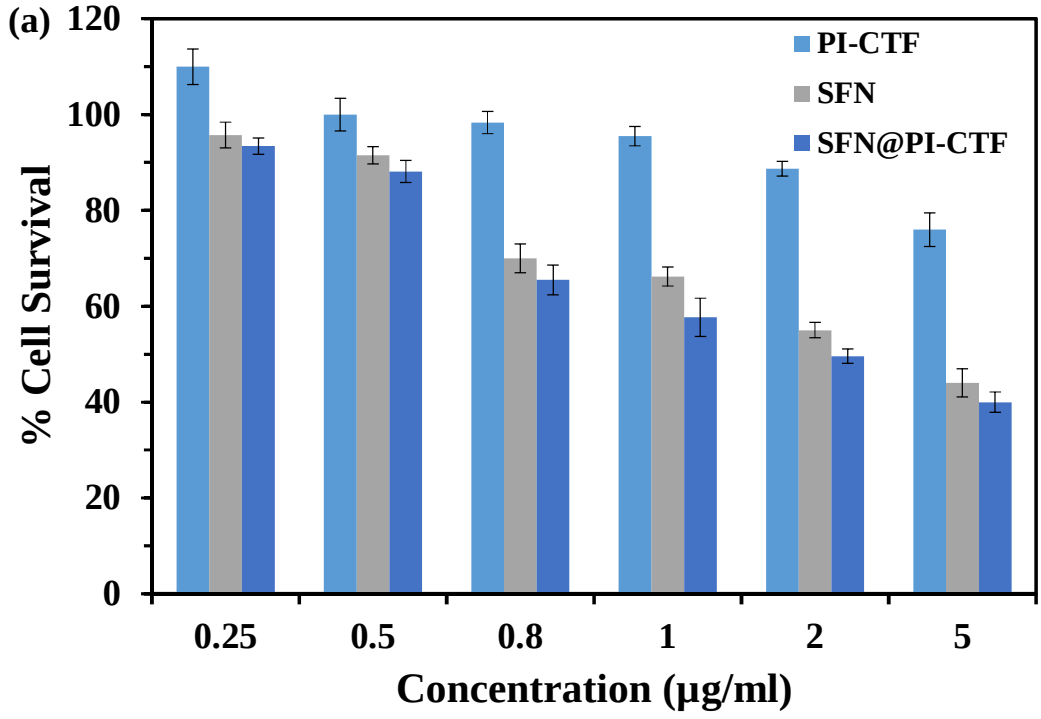

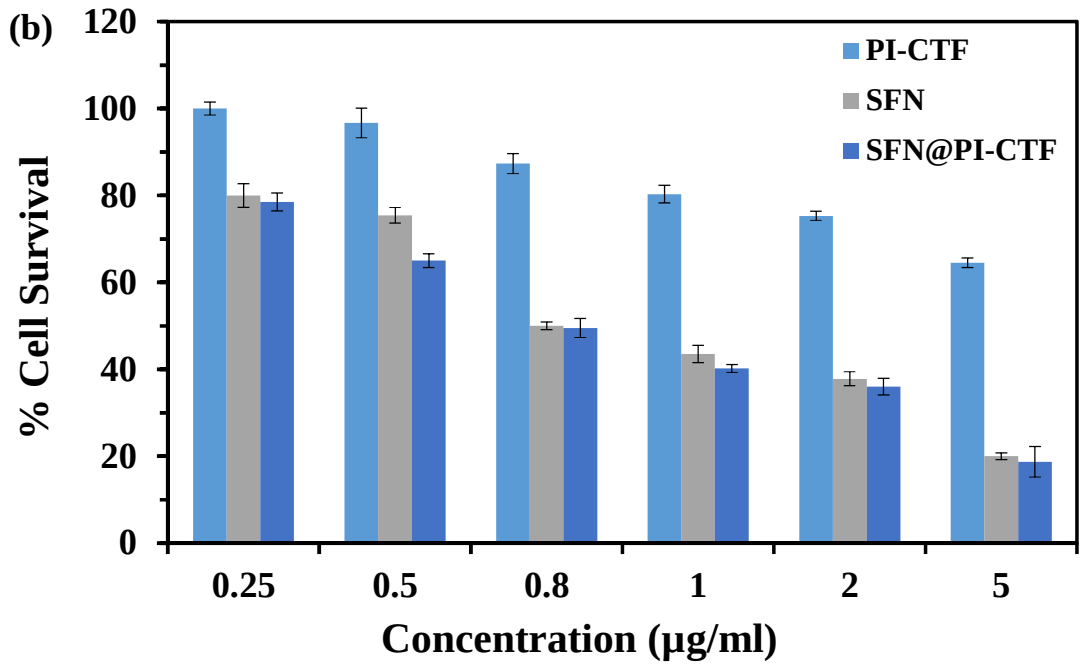

Figure 7. Cytotoxicity of free SFN, SFN@PI-CTF, and PI-CTF against LNCaP cells after (a) 48 and (b) 72 h incubation, respectively.

4. Conclusion

In the present study, TFPTZ was synthesized by simple displacement of chlorine in cyanuric chloride by *p*-hydroxybenzaldehyde and used as a building block for the preparation of PI-CTF by a reaction with hydrazine. Then, the prepared CTF was used as an SFN carrier. Different PI-CTF/drug ratios were studied to find the formulation with the highest encapsulation efficiency and drug loading. *In vitro* cytotoxic study revealed that SFN kept its pharmacological activity when incorporated into PI-CTF. Sustained release of the drug and passive targeting of the PI-CTF to the tumor site may have benefits in reduction of the need to the drug high doses and consequently its fewer side effects. However, further in vivo study is required to confirm the efficacy and side effects of this formulation.

Notes: The authors stated that there are no conflicts of interest in this work.

Acknowledgments

We wish to express our gratitude to the Research Affairs Division Isfahan University of Technology (IUT), Isfahan, for partial financial support.

References

[1] S. Senapati, A.K. Mahanta, S. Kumar, P. Maiti, Controlled drug delivery vehicles for cancer treatment and their performance, Signal transduction and targeted therapy, 3 (2018) 7.

[2] A. Miller, B. Hoogstraten, M. Staquet, A. Winkler, Reporting results of cancer treatment, cancer, 47 (1981) 207-214.

[3] S. Taymouri, J. Varshosaz, The recent progresses on the improved therapy of melanoma by novel drug delivery systems, Current drug targets, 15 (2014) 829-842.

[4] B. Haley, E. Frenkel, Nanoparticles for drug delivery in cancer treatment, Urologic Oncology: Seminars and original investigations, Elsevier, 2008, pp. 57-64.

[5] D. Wu, F. Xu, B. Sun, R. Fu, H. He, K. Matyjaszewski, Design and preparation of porous polymers, Chemical reviews, 112 (2012) 3959-4015.

[6] Y.-R. He, X.-L. Li, X.-L. Li, Z.-Y. Tan, D. Zhang, H.-B. Chen, Aerogel based on melamine-formaldehyde and alginate: Simply removing of uranium from aqueous solutions, Journal of Molecular Liquids, DOI (2019) 111154.

[7] M. Dinari, M. Hatami, Novel N-riched crystalline covalent organic framework as a highly porous adsorbent for effective cadmium removal, Journal of Environmental Chemical Engineering, 7 (2019) 102907.

[8] A. Roy, S. Mondal, A. Halder, A. Banerjee, D. Ghoshal, A. Paul, S. Malik, Benzimidazole linked arylimide based covalent organic framework as gas adsorbing and electrode materials for supercapacitor application, European Polymer Journal, 93 (2017) 448-457.

[9] K.M. Gupta, K. Zhang, J. Jiang, Efficient Removal of Pb2+ from Aqueous Solution by an Ionic Covalent–Organic Framework: Molecular Simulation Study, Industrial & Engineering Chemistry Research, 57 (2018) 6477-6482.

[10] N. Mokhtari, M. Dinari, O. Rahmanian, Novel porous organic triazine-based polyimide with high nitrogen levels for highly efficient removal of Ni (II) from aqueous solution, Polymer International, 68 (2019) 1178-1185.

[11] Z. Babaei, A.N. Chermahini, M. Dinari, M. Saraji, A. Shahvar, A sulfonated triazine-based covalent organic polymer supported on a mesoporous material: a new and robust material for the production of 5-hydroxymethylfurfural, Sustainable Energy & Fuels, 3 (2019) 1024-1032.

[12] F. Su, Q. Jia, Z. Li, M. Wang, L. He, D. Peng, Y. Song, Z. Zhang, S. Fang, Aptamer-templated silver nanoclusters embedded in zirconium metal–organic framework for targeted antitumor drug delivery, Microporous and Mesoporous Materials, 275 (2019) 152-162.

[13] Y. Peng, W.K. Wong, Z. Hu, Y. Cheng, D. Yuan, S.A. Khan, D. Zhao, Room temperature batch and continuous flow synthesis of water-stable covalent organic frameworks (COFs), Chemistry of Materials, 28 (2016) 5095-5101.

[14] F. Haase, E. Troschke, G. Savasci, T. Banerjee, V. Duppel, S. Dörfler, M.M. Grundei, A.M. Burow, C. Ochsenfeld, S. Kaskel, Topochemical conversion of an imine-into a thiazole-linked covalent organic framework enabling real structure analysis, Nature communications, 9 (2018).

[15] L. Bai, S.Z.F. Phua, W.Q. Lim, A. Jana, Z. Luo, H.P. Tham, L. Zhao, Q. Gao, Y. Zhao, Nanoscale covalent organic frameworks as smart carriers for drug delivery, Chemical Communications, 52 (2016) 4128-4131.

[16] G.K. Abou-Alfa, L. Schwartz, S. Ricci, D. Amadori, A. Santoro, A. Figer, J. De Greve, J.-Y. Douillard, C. Lathia, B. Schwartz, Phase II study of sorafenib in patients with advanced hepatocellular carcinoma, Journal of Clinical Oncology, 24 (2006) 4293-4300.

[17] R.K. Thapa, J.Y. Choi, B.K. Poudel, T.T. Hiep, S. Pathak, B. Gupta, H.-G. Choi, C.S. Yong, J.O. Kim, Multilayer-coated liquid crystalline nanoparticles for effective sorafenib delivery to hepatocellular carcinoma, ACS applied materials & interfaces, 7 (2015) 20360-20368.

[18] C. Gridelli, P. Maione, F. Del Gaizo, G. Colantuoni, C. Guerriero, C. Ferrara, D. Nicolella, D. Comunale, A. De Vita, A. Rossi, Sorafenib and sunitinib in the treatment of advanced non-small cell lung cancer, The oncologist, 12 (2007) 191-200.

[19] C. Fumarola, C. Caffarra, S. La Monica, M. Galetti, R.R. Alfieri, A. Cavazzoni, E. Galvani, D. Generali, P.G. Petronini, M.A. Bonelli, Effects of sorafenib on energy metabolism in breast cancer cells: role of AMPK–mTORC1 signaling, Breast cancer research and treatment, 141 (2013) 67-78.

[20] M. Tran, A. Sharma, C. Smith, M. Kester, G. Robertson, A combinatorial approach using sorafenib and liposomal ceramide to inhibit malignant melanoma, AACR, 2007.

[21] S. Wilhelm, C. Carter, M. Lynch, T. Lowinger, J. Dumas, R.A. Smith, B. Schwartz, R. Simantov, S. Kelley, Discovery and development of sorafenib: a multikinase inhibitor for treating cancer, Nature reviews Drug discovery, 5 (2006) 835.

[22] U. Srimathi, V. Nagarajan, R. Chandiramouli, Investigation on graphdiyne nanosheet in adsorption of sorafenib and regorafenib drugs: a DFT approach, Journal of Molecular Liquids, 277 (2019) 776-785.

[23] A. Ullén, M. Farnebo, L. Thyrell, S. Mahmoudi, P. Kharaziha, L. Lennartsson, D. Grandér, T. Panaretakis, S. Nilsson, Sorafenib induces apoptosis and autophagy in prostate cancer cells in vitro, International journal of oncology, 37 (2010) 15-20.

[24] M.L. Bondì, C. Botto, E. Amore, M.R. Emma, G. Augello, E.F. Craparo, M. Cervello, Lipid nanocarriers containing sorafenib inhibit colonies formation in human hepatocarcinoma cells, International journal of pharmaceutics, 493 (2015) 75-85.

[25] F.G. Khan, M.V. Yadav, A.D. Sagar, Synthesis, characterization, and antimicrobial evaluation of novel trichalcones containing core s-triazine moiety, Medicinal Chemistry Research, 23 (2014) 2633-2638.

[26] V.A.d. Mello, E. Ricci-Júnior, Encapsulation of naproxen in nanostructured system: structural characterization and in vitro release studies, Quimica Nova, 34 (2011) 933-939.

[27] Z. Li, X. Feng, Y. Zou, Y. Zhang, H. Xia, X. Liu, Y. Mu, A 2D azine-linked covalent organic framework for gas storage applications, Chemical Communications, 50 (2014) 13825-13828.

[28] D.W. van Krevelen, Properties of Polymers: Their Estimation and Correlation with Chem. Structure, Elsevier Scientific Publ.1976.

[29] B.W. Liu, L. Chen, D.M. Guo, X.F. Liu, Y.F. Lei, X.M. Ding, Y.Z. Wang, Fire-Safe Polyesters Enabled by End-Group Capturing Chemistry, Angewandte Chemie International Edition, 58 (2019) 9188-9193.

[30] A. Schirp, A. Hellmann, Fire retardancy improvement of high-density polyethylene composites based on thermomechanical pulp treated with ammonium polyphosphate, Polymer Composites, 40 (2019) 2410-2423.

[31] Y. Huang, S. Jiang, R. Liang, Z. Liao, G. You, A green highly-effective surface flame-retardant strategy for rigid polyurethane foam: transforming UV-cured coating into intumescent self-extinguishing layer, Composites Part A: Applied Science and Manufacturing, DOI (2019) 105534.

[32] Y. Zhang, Z. Zhi, T. Jiang, J. Zhang, Z. Wang, S. Wang, Spherical mesoporous silica nanoparticles for loading and release of the poorly water-soluble drug telmisartan, Journal of Controlled Release, 145 (2010) 257-263.

[33] H. Radhouani, D. Bicho, C. Gonçalves, F.R. Maia, R.L. Reis, J.M. Oliveira, Kefiran cryogels as potential scaffolds for drug delivery and tissue engineering applications, Materials Today Communications, DOI (2019) 100554.

[34] J.E. Brown, L. Tozzi, B. Schilling, A. Kelmendi-Doko, A.B. Truong, M.J. Rodriguez, E.S. Gil, R. Sucsy, J.E. Valentin, B.J. Philips, Biodegradable silk catheters for the delivery of therapeutics across anatomical repair sites, Journal of Biomedical Materials Research Part B: Applied Biomaterials, 107 (2019) 501-510.

[35] Y.-C. Yang, J. Cai, J. Yin, J. Zhang, K.-L. Wang, Z.-T. Zhang, Heparin-functionalized Pluronic nanoparticles to enhance the antitumor efficacy of sorafenib in gastric cancers, Carbohydrate polymers, 136 (2016) 782-790.

[36] P. Xu, E.A. Van Kirk, W.J. Murdoch, Y. Zhan, D.D. Isaak, M. Radosz, Y. Shen, Anticancer efficacies of cisplatin-releasing pH-responsive nanoparticles, Biomacromolecules, 7 (2006) 829-835.

[37] J. Varshosaz, F. Hassanzadeh, H. Sadeghi-Aliabadi, Z. Larian, M. Rostami, Synthesis of Pluronic® F127-poly (methyl vinyl ether-alt-maleic acid) copolymer and production of its micelles for doxorubicin delivery in breast cancer, Chemical Engineering Journal, 240 (2014) 133-146.

[38] J. Varshosaz, S. Taymouri, F. Hassanzadeh, S.H. Javanmard, M. Rostami, Self-assembly micelles with lipid core of cholesterol for docetaxel delivery to B16F10 melanoma and HepG2 cells, Journal of liposome research, 25 (2015) 157-165.

[39] E.K. Park, S.Y. Kim, S.B. Lee, Y.M. Lee, Folate-conjugated methoxy poly (ethylene glycol)/poly (ε-caprolactone) amphiphilic block copolymeric micelles for tumor-targeted drug delivery, Journal of Controlled Release, 109 (2005) 158-168.

[40] L. Chen, X. Sha, X. Jiang, Y. Chen, Q. Ren, X. Fang, Pluronic P105/F127 mixed micelles for the delivery of docetaxel against Taxol-resistant non-small cell lung cancer: optimization and in vitro, in vivo evaluation, International journal of nanomedicine, 8 (2013) 73.

[41] A.K. Mohanty, F. Dilnawaz, C. Mohanty, S.K. Sahoo, Etoposide-loaded biodegradable amphiphilic methoxy (poly ethylene glycol) and poly (epsilon caprolactone) copolymeric micelles as drug delivery vehicle for cancer therapy, Drug delivery, 17 (2010) 330-342.

[42] M. Moezzi, A. Mohebbi, A. Pardakhti, Preparation of niosomes containing sorafenib and evaluation of their physicochemical properties, Peer-review multidisciplinary pharmacy scientific journal, 1 84.

[43] H. Liu, S. Wu, J. Yu, D. Fan, J. Ren, L. Zhang, J. Zhao, Reduction-sensitive micelles self-assembled from amphiphilic chondroitin sulfate A-deoxycholic acid conjugate for triggered release of doxorubicin, Materials Science and Engineering: C, 75 (2017) 55-63.

[44] S. Park, H.S. Yoo, In vivo and in vitro anti-cancer activities and enhanced cellular uptakes of EGF fragment decorated doxorubicin nano-aggregates, International journal of pharmaceutics, 383 (2010) 178-185.

[45] H. Lian, Y. Du, X. Chen, L. Duan, G. Gao, C. Xiao, X. Zhuang, Core cross-linked poly (ethylene glycol)-graft-Dextran nanoparticles for reduction and pH dual responsive intracellular drug delivery, Journal of colloid and interface science, 496 (2017) 201-210.

[46] Q. Liu, R. Li, Z. Zhu, X. Qian, W. Guan, L. Yu, M. Yang, X. Jiang, B. Liu, Enhanced antitumor efficacy, biodistribution and penetration of docetaxel-loaded biodegradable nanoparticles, International journal of pharmaceutics, 430 (2012) 350-358.

[47] X. Wang, Y. Wang, X. Chen, J. Wang, X. Zhang, Q. Zhang, NGR-modified micelles enhance their interaction with CD13-overexpressing tumor and endothelial cells, Journal of Controlled Release, 139 (2009) 56-62.

[48] D.-H. Seo, Y.-I. Jeong, D.-G. Kim, M.-J. Jang, M.-K. Jang, J.-W. Nah, Methotrexate-incorporated polymeric nanoparticles of methoxy poly (ethylene glycol)-grafted chitosan, Colloids and Surfaces B: Biointerfaces, 69 (2009) 157-163.

[49] Z. Zhang, S.-S. Feng, The drug encapsulation efficiency, in vitro drug release, cellular uptake and cytotoxicity of paclitaxel-loaded poly (lactide)–tocopheryl polyethylene glycol succinate nanoparticles, Biomaterials, 27 (2006) 4025-4033.

[50] N. Sepehri, H. Rouhani, F. Tavassolian, H. Montazeri, M.R. Khoshayand, M.H. Ghahremani, S.N. Ostad, F. Atyabi, R. Dinarvand, SN38 polymeric nanoparticles: in vitro

cytotoxicity and in vivo antitumor efficacy in xenograft balb/c model with breast cancer versus irinotecan, International journal of pharmaceutics, 471 (2014) 485-497.

- Novel covalent triazine-based polyimine framework (PI-CTF) with good biocompatibility was synthesized
- PI-CTF show good efficacy with drug loading of 83% for sorafenib (SFN) delivery
- The *in vitro* release study showed a sustained and pH-dependent release behavior

- Cytotoxicity assay against L929 cells revealed these nanocarriers were safe and biocompatible structures

Dear Editor;

Title: Covalent triazine-based polyimine framework as a biocompatible nanocarrier for sorafenib with the sustained and pH-dependent release: an in vitro approach

By myself and co-authours for possible publication in one of the forthcoming volumes of **Journal of Molecular Liquids**.

This manuscript is original, has not been published elsewhere, has not been published previously, is not under consideration for publication elsewhere and our intent is to publish in the Journal of Molecular Liquids.

Hereby, also in behalf of my co-authors, would like to submit this manuscript for publication in the Journal of Molecular Liquids**.**

Also, no conflict of interest exists and if accepted, the article will not be published elsewhere in the same form, in any language, without the written consent of the publisher.

Regards;

Dr. M. Dinari

Associate Prof. of Organic Polymer Chemistry

Department of Chemistry

Isfahan University of Technology, Isfahan, 84156-83111, I.R. Iran

Tel: ++98-31-3391-3270; Fax: ++98-31-3391-2350

Other e-mail: mdinary@gmail.com; mdinary@ch.iut.ac.ir